Determination of the magnetization distribution in Cr_2O_3 using spherical neutron polarimetry

2002 J. Phys.: Condens. Matter 14 1957

(http://iopscience.iop.org/0953-8984/14/8/323)

INSTITUTE OF PHYSICS PUBLISHING JOURNAL OF PHYSICS: CONDENSED MATTER

J. Phys.: Condens. Matter **14** (2002) 1957–1966 PII: S0953-8984(02)24287-3

Determination of the magnetization distribution in Cr_2O_3 using spherical neutron polarimetry

P J Brown[1,2], J B Forsyth[3], E Lelièvre-Berna[1] and F Tasset[1]

[1] Institut Laue Langevin, BP 156 38042 Grenoble Cedex, France
[2] Department of Physics, Loughborough University, Loughborough LE11 3TU, UK
[3] ISIS Department, Rutherford Appleton Laboratory, Chilton, Oxon OX11 0QX, UK

Received 26 April 2001, in final form 12 November 2001
Published 15 February 2002
Online at stacks.iop.org/JPhysCM/14/1957

Abstract

The magnetization distribution due to the Cr^{3+} ion in Cr_2O_3 has been determined using spherical neutron polarimetry. The magnetic structure factors of $h\ 0\ l$ reflections have been measured out to $\sin\theta/\lambda = 0.75\ \text{Å}^{-1}$. The results show that the Cr^{3+} magnetic moment is reduced by the zero-point spin deviation and by covalent mixing to 2.48 μ_B. They are consistent with the Cr d electrons being in the trigonally symmetric a_1 and e orbitals derived from the cubic orbitals with t_{2g} symmetry. There is a small but significant magnetization which is not accounted for by these orbitals, which is attributed to covalent overlap. Its symmetry is consistent with the magneto-electric susceptibility.

1. Introduction

The classical polarized neutron diffraction technique [1] has been extensively used to study the magnetization distribution around magnetic atoms and ions in ferromagnetic and paramagnetic materials. In favourable cases very precise results can be obtained [2]. It is very much more difficult to make such measurements in antiferromagnetic systems because in antiferromagnets the cross-section is not often polarization dependent, so the classical method is not applicable. As a consequence, very few measurements of the magnetization distribution in antiferromagnetic materials have been made, since usually they require very precise integrated intensity measurements of rather weak reflections. In the few cases where such measurements have been undertaken they have given very interesting results [3–5]. An antiferromagnetic magnetization distribution is more sensitive than a ferromagnetic or paramagnetic one to the effects of covalency because the overlap of positive and negative transferred spin on the ligand ions leads to an actual loss of moment rather than just to a redistribution. Up to now no precise measurements have been made in antiferromagnetic structures with zero propagation vector and in which magnetic atoms of opposite spin are related by a centre of symmetry. In such structures the magnetic and nuclear scattering are superimposed, making separation of the nuclear and magnetic parts difficult. Additionally, the

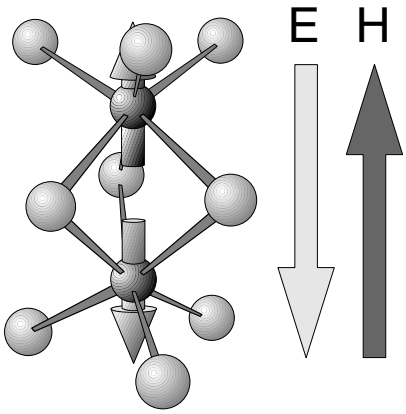

Figure 1. The oxygen coordination polyhedron surrounding a pair of oppositely directed Cr^{3+} ions in Cr_2O_3. It consists of two octahedra sharing a triangular face. The spin directions shown are those stabilized by cooling in antiparallel fields as indicated by the arrows.

Table 1. Crystallographic data for Cr_2O_3.

Space group:	$R\bar{3}c$	Hexagonal axes	
Unit cell:	$a = 4.9607$ Å	$c = 13.599$ Å	
Atomic positions:	12 Cr in 12 (c)	0 0 z	$z = 0.3476$
	18 O in 18 (e)	x 0 $\frac{1}{4}$	$x = 0.3056$

magnetic and nuclear structure factors are in phase quadrature, so there can be no interference between them to give a polarization-dependent cross-section. The newly developed technique of spherical neutron polarimetry (SNP) [6] allows a precise measurement of the magnetic scattering in such structures, and this can be exploited to determine the antiferromagnetic magnetization distribution.

Cr_2O_3 belongs to the class of antiferromagnets introduced above whose magnetic structure factors can be measured using SNP. It crystallizes with the corundum structure in which the chromium is octahedrally coordinated by oxygen atoms (the structural details are given in table 1). The Cr sites are not centres of symmetry, so the triad axis of the octahedron is polar. Below 310 K the Cr^{3+} ions order antiferromagnetically and the material exhibits a magnetoelectric (ME) effect. The Cr^{3+} spins are aligned parallel to the triad axis, ions with opposite spins being related by the centres of symmetry and by the diad axes parallel to $\langle 1\ 0\ 0 \rangle$ [15]. In this structure 180° domains can occur, which are distinguished by the direction in which the spins point relative to the polar axis of their coordinating octahedron. We have shown in a previous study [8] that a crystal consisting of essentially a single 180° domain can be prepared by cooling the sample through its Néel point, in a combination of magnetic and electric fields applied along the triad axis. Figure 1 shows the spin configuration of the double octahedral complex, which is stabilized by cooling in oppositely directed electric and magnetic fields parallel and antiparallel to [0 0 1].

2. Neutron polarimetry

The SNP technique has been described in several publications [6, 7] and an outline of its use to determine accurate values of magnetic structure factors is given in [9]. As shown there, the

results of such experiments can be described by the tensor equation

$$P_i' = \mathbf{P}_{ij} P_j + P_j'' \tag{1}$$

where $\mathbf{P}$ is a tensor describing the rotation of the polarization in the scattering process and $\boldsymbol{P}''$ is the polarization created. For a magnetic structure in which the magnetic and nuclear scattering occur in the same reflections and are in phase quadrature $\boldsymbol{P}'' = 0$.

We define the magnetic structure factors $\boldsymbol{M}(\boldsymbol{k})$ in terms of the Fourier transform of the magnetization distribution $\boldsymbol{M}(\boldsymbol{r})$, and the *magnetic interaction vector* $\boldsymbol{M}_\perp(\boldsymbol{k})$ as the projection of $\boldsymbol{M}(\boldsymbol{k})$ on the plane perpendicular to the scattering vector $\boldsymbol{k}$:

$$\boldsymbol{M}(\boldsymbol{k}) = \int \boldsymbol{M}(\boldsymbol{r}) \exp(\mathrm{i}\boldsymbol{k} \cdot \boldsymbol{r})\, \mathrm{d}r^3 \tag{2}$$

$$\boldsymbol{M}_\perp(\boldsymbol{k}) = \hat{\boldsymbol{k}} \times \boldsymbol{M}(\boldsymbol{k}) \times \hat{\boldsymbol{k}} \tag{3}$$

where $\hat{\boldsymbol{k}}$ is a unit vector parallel to $\boldsymbol{k}$. For centrosymmetric structures, the origin may be chosen to make the nuclear structure factors $N(\boldsymbol{k})$ real and the magnetic interaction vectors $\boldsymbol{M}_\perp(\boldsymbol{k})$ imaginary. In this case, a ratio of magnetic to nuclear scattering γ can be defined as $\gamma = \boldsymbol{M}_\perp(\boldsymbol{k}) \cdot \hat{\boldsymbol{M}}_\perp(\boldsymbol{k})/\mathrm{i}N(\boldsymbol{k})$, where $\hat{\boldsymbol{M}}_\perp(\boldsymbol{k})$ is a unit vector parallel to $\boldsymbol{M}_\perp(\boldsymbol{k})$.

It is useful to define *polarization axes* with $\boldsymbol{x}$ parallel to the scattering vector $\boldsymbol{k}$, $\boldsymbol{z}$ vertical, and $\boldsymbol{y}$ completing the right handed orthogonal set. Then, when the moment direction lies in the $\boldsymbol{x}$–$\boldsymbol{y}$ plane as in this experiment,

$$\begin{array}{lll} \mathbf{P}_{xx} = \beta & \mathbf{P}_{xy} = 0 & \mathbf{P}_{xz} = \xi \\ \mathbf{P}_{yx} = 0 & \mathbf{P}_{yy} = 1 & \mathbf{P}_{yz} = 0 \\ \mathbf{P}_{zx} = -\xi & \mathbf{P}_{zy} = 0 & \mathbf{P}_{zz} = \beta \end{array} \tag{4}$$

$$\text{with} \quad \xi = \frac{2\epsilon\gamma}{1+\gamma^2} \qquad \text{and} \qquad \beta = \frac{1-\gamma^2}{1+\gamma^2}. \tag{5}$$

ϵ is +1 if $\hat{\boldsymbol{M}}_\perp(\boldsymbol{k})$ is parallel to $\boldsymbol{y}$ and −1 if it is antiparallel. γ has opposite signs for the two 180° domains, so the final polarization is the result of summing the scattered polarization, weighted by its intensity, over the two domains. If the domain imbalance ratio is $\eta = (v^+ - v^-)/(v^+ + v^-)$ where v^+ and v^- are the volumes of crystal belonging to the two domains, the resultant polarization matrix has the same form as that of equation 4 except that the terms in ξ are multiplied by η, giving

$$\boldsymbol{P}_{xz} = -\boldsymbol{P}_{zx} = \eta\xi. \tag{6}$$

For an equi-domain crystal $\eta = 0$, the matrix is diagonal and the incident and scattered polarizations are always parallel. Depolarization by the factor β occurs for incident polarization parallel to either $\boldsymbol{x}$ or $\boldsymbol{z}$, but a beam polarized parallel to $\boldsymbol{y}$ (the direction of the interaction vector) is always scattered without change of polarization. Each reflection for which the full polarization matrix is determined gives four independent estimates of γ, two of which, those from $\boldsymbol{P}_{xx}$ and $\boldsymbol{P}_{zz}$, are independent of η. $\boldsymbol{P}_{xz}$ and $\boldsymbol{P}_{zx}$ give estimates which, even though they depend on η, will give a more precise determination of γ if η is non-zero and $|\gamma| \ll 1$.

3. Polarimetric measurements

Measurements have been made on Cr_2O_3 at 24 K of reflections of the form $h\ 0\ l$ with l even; those with l odd are systematically absent. In the experiments reported in [9] the reflections with $\sin\theta/\lambda < 0.5$ Å^{-1} were measured by determining the full polarization matrix. Two different crystals were used; the first was measured in three, and the second in two, different

domain states. The values of γ obtained for the same reflections of all five sets were in good agreement, leading to rather precise values of the magnetic interaction vectors. These data were measured with CRYOPAD installed on the polarized triple axis spectrometer IN20 at ILL and the extent of the data measured was limited by geometrical constraints.

It has recently become possible to extend these measurements to higher momentum transfer by installing CRYOPAD on the hot-source polarized neutron diffractometer D3 at ILL and using the newly available ^{3}He neutron spin filter to allow polarization analysis of the diffracted beam [10]. At the higher $\sin\theta/\lambda$ values the magnetic scattering becomes very weak and it is impractical to measure all components of the polarization matrix. However, if the domain ratio is high and is determined using the lower-angle reflections, then it is sufficient to measure just the P_{xz} and P_{zx} components. These are linearly rather than quadratically dependent on γ and may be corrected for deficiencies in the transmitted polarization using the P_{yy} component. Using this method we were able to measure the magnetic structure factors of 14 h 0 l reflections with $\sin\theta/\lambda$ between 0.5 and 0.75 Å^{-1} on a crystal which had been field cooled to give a domain ratio $\eta = 0.943(9)$.

4. Analysis of the data

Although the data measured in these experiments are the ratios between the magnetic interaction vectors and the nuclear structure factors, they can be displayed in a first analysis as a magnetic form factor for the Cr^{3+} ion. If the magnetic scattering from Cr_2O_3 is described by a magnetic moment $\boldsymbol{m}$ with a form factor $f(\boldsymbol{k})$ then the magnetic structure factor can be written

$$\boldsymbol{M}(\boldsymbol{k}) = 12\boldsymbol{m}f(\boldsymbol{k})\mathrm{i}\sin(k_z z_{\mathrm{Cr}}) \tag{7}$$

and

$$|\boldsymbol{m}|f(\boldsymbol{k}) = \gamma N(\boldsymbol{k})/\,(12\sin\alpha\,\sin\,(k_z z_{\mathrm{Cr}})) \tag{8}$$

where α is the angle between $\boldsymbol{M}(\boldsymbol{k})$ and $\boldsymbol{k}$. Table 2 shows the measured gamma values, and the magnetic structure factors and form factors deduced from them using the above equations. It can be seen that the precision obtained is very good except for the few cases where either the nuclear structure factor $N(\boldsymbol{k})$ is very large or one of the geometric factors $\sin(k_z z_{\mathrm{Cr}})$ or $\sin\alpha$ is small. The values of the form factor deduced in this way for each of the Bragg reflections measured are plotted in figure 2, where they are compared with the Cr^{3+} form factor normalized to the lowest-angle reflection (1 0 2).

The most significant result of this analysis is the low value of the Cr^{3+} moment, 2.5 μ_{B} required to fit the Cr^{3+} form factor to the 1 0 2 reflection. Magnetic resonance studies of Cr^{3+} ions in Al_2O_3 give a g-factor of 1.98, leading to a moment of 2.97 μ_{B} [12].

5. Multipole analysis

The Cr^{3+} ion in Cr_2O_3 lies on a triad axis but has no other symmetry. The real combinations of even multipole functions permitted by this symmetry up to order four are

$$\begin{aligned} &Y(00) = Y_0^0, \qquad Y(20) = Y_2^0, \qquad Y(40) = Y_4^0, \\ &Y(43+) = \frac{1}{\mathrm{i}\sqrt{2}}(Y_4^{-3} + Y_4^3) \qquad \text{and} \qquad Y(43-) = \frac{1}{\sqrt{2}}(Y_4^3 - Y_4^{-3}). \end{aligned} \tag{9}$$

In the present experiment we have measured only h 0 l reflections so only one of the combinations $Y(43+)$, $Y(43-)$ can be determined; if x is parallel to a^* it is $Y(43-)$. The amplitudes of the four allowed functions were varied in a multipole refinement using the

Table 2. Values of γ and $M_c(\boldsymbol{k})$ measured for the $h\ 0\ l$ reflections of Cr_2O_3 compared with those calculated for the spherical and multipole models. The magnetic structure factors are all parallel or antiparallel to the $\boldsymbol{c}$-axis ([0 0 1]) and are given in μ_B per hexagonal unit cell.

hkl	$\sin\theta/\lambda$ Å^{-1}	γ_{obs}	$M_c(\boldsymbol{k})_{obs}$	$M_c(\boldsymbol{k})_{sph}$ [a]	$M_c(\boldsymbol{k})_{t2g}$ [b]
1 0 2	0.1377	2.033(8)	−22.88(9)	−22.96	−22.96
1 0 $\bar{4}$	0.1875	1.000(3)	−13.52(4)	−13.17	−13.15
2 0 $\bar{2}$	0.2441	10.02(78)	14.18(111)	15.41	15.44
2 0 4	0.2753	−0.386(3)	8.72(5)	8.95	8.86
1 0 8	0.3163	−0.60(2)	−11.57(35)	−11.09	−11.37
2 0 $\bar{8}$	0.3751	−1.00(1)	5.78(8)	7.79	7.52
1 0 $\bar{10}$	0.3857	0.020(6)	−1.30(39)	−1.12	−1.21
3 0 $\bar{6}$	0.4130	−0.085(5)	−2.51(12)	3.16	2.96
3 0 6	0.4130	0.105(5)	2.03(12)	−3.16	−2.96
2 0 10	0.4352	−0.042(5)	0.71(8)	0.80	0.78
4 0 2	0.4713	0.158(5)	−3.48(11)	−3.79	−4.18
4 0 $\bar{4}$	0.4882	−0.56(2)	−2.49(8)	−2.24	−2.31
1 0 14	0.5277	−0.076(4)	−2.26(11)	−1.88	−2.80
4 0 8	0.5507	−0.046(3)	−1.03(7)	−2.00	−1.45
3 0 $\bar{12}$	0.5626	−0.003(5)	−0.22(30)	−1.60	−1.19
3 0 12	0.5626	0.023(5)	1.46(34)	1.60	1.19
2 0 $\bar{14}$	0.5649	0.055(3)	2.22(12)	1.32	1.67
5 0 $\bar{2}$	0.5866	0.230(10)	1.45(6)	1.34	1.85
4 0 $\bar{10}$	0.5932	0.019(3)	−0.74(11)	−0.20	−0.09
1 0 $\bar{16}$	0.5997	−0.009(2)	0.50(12)	0.46	1.00
5 0 4	0.6002	−0.024(5)	0.59(13)	0.78	0.96
2 0 16	0.6327	0.009(3)	−0.49(15)	−0.31	−0.57
5 0 $\bar{8}$	0.6520	−0.05(2)	0.43(17)	0.60	0.24
4 0 14	0.6940	−0.10(2)	0.82(18)	−0.20	0.28
6 0 0	0.6983	0.011(3)	0.41(11)	0.00	0.00
6 0 6	0.7323	0.05(1)	−0.47(13)	0.02	0.08
1 0 20	0.7445	0.003(5)	0.36(57)	0.01	−0.45

[a] Calculated for 2.47 μ_B/Cr^{3+} with spherical free ion form factor [11].
[b] Calculated for 2.48 μ_B/Cr^{3+} in the a_1 + 2e orbitals of equation (12).

observed magnetic structure factors as data. The only significant amplitudes determined were $Y(00) = 2.48(3)$ and $Y(40) = 0.54(20)$.

The ground state of the free Cr^{3+} ion (d^3) is ^4F, which is split by an octahedral field into an orbital singlet ground state $^4A_2$ and two orbital triplets $^4T_2$ and $^4T_1$, the first of which can be mixed with the ground state by spin–orbit coupling. As mentioned above, this mixing is thought to be very small. In the $^4A_2$ ground state all three d electrons have parallel spins and occupy the three t_{2g} states. These three states are split by the trigonal field into a singly degenerate state with a_1 symmetry and a doubly degenerate pair with e symmetry. They may be written

$$\begin{aligned} a_1 &= Y_2^0 \\ e_1 &= [\sqrt{2}(Y_2^{-2} + Y_2^2) - i(Y_2^{-1} + Y_2^1)]/\sqrt{6} \\ e_2 &= [\sqrt{2}i(Y_2^{-2} - Y_2^{+2}) - (Y_2^{-1} - Y_2^{+1})]/\sqrt{6} \end{aligned} \tag{10}$$

the corresponding densities are

$$\begin{aligned} |a_1|^2 &= Y(00) + \frac{\sqrt{20}}{7}Y(20) + \frac{6}{7}Y(40) \\ \frac{1}{2}(|e_1|^2 + |e_2|^2) &= Y(00) - \frac{\sqrt{5}}{7}Y(20) - \frac{2}{21}Y(40) + \sqrt{\frac{20}{63}}Y(43+) \end{aligned} \tag{11}$$

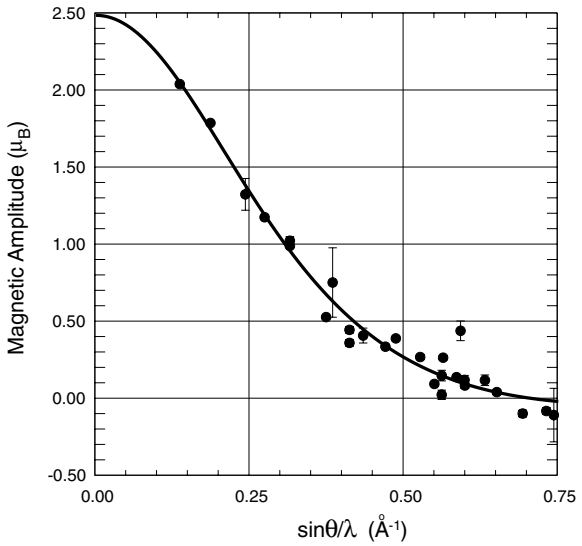

Figure 2. The magnetic scattering per Cr^{3+} ion corresponding to the magnetic structure factors measured for the $h\ 0\ l$ relections of Cr_2O_3 plotted versus $\sin\theta/\lambda$. The full curve is the Cr^{3+} free ion form factor calculated from the radial wavefunctions given by [11].

and the sum over the three states is

$$3|(t_{2g}|^2) = 3Y(00) + \tfrac{2}{3}Y(40) + \tfrac{4}{3}\sqrt{\tfrac{5}{7}}Y(43+). \tag{12}$$

The results of the multipole refinement are consistent with this configuration, but the observed amplitudes of $Y(00)$ and $Y(40)$ compared with those in equation (12) indicate a moment reduction of about 20%. The absence of a significant amplitude for $Y(20)$ $(-0.02(9))$ shows that the a_1 and the doubly degenerate e states are equally occupied and the overall t_{2g} symmetry conserved.

6. Maximum-entropy reconstruction

A maximum-entropy map of the difference between the observations and a model consisting of 2.48 Cr 3d electrons in the three trigonal orbitals derived from the cubic t_{2g} states was constructed [14]. The routines used by the maximum-entropy algorithm to transform between real and reciprocal space were modified to take into account the antiferromagnetic symmetry of Cr_2O_3. Although data are only available for $h\ 0\ l$ reflections the trigonal symmetry can be used to expand them into a quasi-three dimensional set. Figure 3 shows a section of the maximum-entropy (MAXE) reconstruction perpendicular to [0 1 0] passing through the origin. This section was chosen because it contains all the significant features of the complete reconstruction. The antisymmetry appropriate to the antiferromagnetic structure can be clearly seen. The most prominent features of the map are regions of positive density close to the Cr sites with positive spin, paired with equivalent regions of negative density close to those with negative spin. The Cr^{3+} ion itself is at a position where there is a magnetization gradient. The most significant peaks in the difference map occur at a distance around 0.7 Å from the Cr site. It is at about this distance that the maximum in the overlap between the radial wavefunctions for Cr^{3+} and the O^{2-} ions of the coordination octahedron occurs, so it is tempting to ascribe these features to covalent overlap.

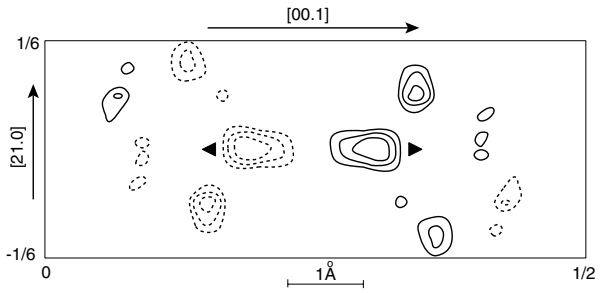

Figure 3. Maximum-entropy reconstruction of the density corresponding to the difference between the observed magnetization distribution and that calculated from the multipole model of equation (12). The section shown is perpendicular to [0 1 0] and passes through the origin. The contours are logarithmically spaced with a factor of two between successive levels. The highest contour is at 1.0 μ_B Å^{-3}; negative contours are dashed. The filled triangles mark the Cr^{3+} ion positions; the one farthest to the right in the diagram has positive spin.

7. Discussion

SNP has enabled a precise value for the sublattice magnetization in Cr_2O_3 to be determined for the first time, since the accuracy of the values obtained from integrated intensity measurements is limited because of the superposition of nuclear and magnetic scattering. An early determination using a powder sample gave a value of 2.76(3) [15] which is significantly greater than that obtained here. Their value depends on the comparison of data collected at different temperatures, and it is difficult to pin-point possible sources of systematic error since the original data are not available. Moreover, the precise method of analysis is not given in the publication, neither are the nuclear scattering lengths nor the source of the Mn^{2+} magnetic form factor adopted. With SNP the rotation of the polarization is measured with constant cross-section and so is not affected by extinction, and the ratio of nuclear to magnetic scattering is obtained without changing the experimental conditions. The reproducibility of the method is demonstrated by the agreement between the results obtained for two different crystals and with different degrees of domain imbalance. In the present experiment the precision with which the sub-lattice magnetization can be determined depends rather more on the precision of the assumed form-factor than on that of the measurements. The multipole fit gives a sublattice magnetization of 2.48(3) μ_B.

The exchange interactions in Cr_2O_3 have been determined using inelastic neutron scattering [16]. The spin-wave spectra could be fitted with a Heisenberg Hamiltonian including neighbours out to about 6.1 Å although only the interactions between first and second neighbours were strong ($J_1 \approx 2J_2 \approx 25J_3$). Using the Heisenberg Hamiltonian the value of $\langle S_z \rangle$ at $T = 0$ was calculated to be 1.38, giving a zero-point spin deviation of 8%. This would reduce the expected Cr moment to 2.73 μ_B, so some half of the moment deficit found in the present experiment may be due to zero-point spin deviation, but the other half must be sought elsewhere.

A moment deficit is not unexpected in antiferromagnetic salts, where covalent mixing between the metal ion and its ligands can lead to cancellation between positive and negative magnetization transferred to the ligand sites [13].

The antiferromagnetic structure of Cr_2O_3 is such that each O^{2-} ion has two Cr^{3+} neighbours with positive and with negative spin. In a molecular orbital model the singly occupied states will be those antibonding orbitals of π character in which the trigonal orbitals derived from the

cubic t_{2g} states of Cr^{3+} are mixed with oxygen p functions. Such mixing transfers spin from the Cr^{3+} to the O^{2-} ions, but each O^{2-} ion gains as much positive spin from its two positive neighbours as negative spin from its two negative neighbours, so there is no net magnetization associated with the O^{2-} ions. The only effect of the covalent mixing on the magnetization distribution is to lower the moment on the Cr^{3+} site and to introduce extra magnetization in regions where there is strong overlap between the Cr^{3+} and O^{2-} wavefunctions. The covalent mixing parameter can be calculated roughly from the moment deficit assuming orbitals of the form [13]

$$\psi = N(\psi_d + \lambda\psi_p) \tag{13}$$

where ψ_d and ψ_p are orbital wavefunctions for the Cr^{3+} 3d and O^{2-} 2p electrons respectively. The corresponding density is

$$\psi\psi^* = N^2(\psi_d\psi_d^* + 2\mathrm{Re}\,(\lambda\psi_d\psi_p^*) + \lambda^2\psi_p\psi_p^*). \tag{14}$$

Although this is a simplified description, it is appropriate to Cr_2O_3 since the a_1 and the doubly degenerate e states are equally occupied and each orbital interacts with six oxygen ions. There are six equivalent Cr^{3+} ions of each spin state and 18 equivalent O^{2-} ions in the hexagonal unit cell. Then, if the wavefunctions are suitably symmetrized, the integral of the density corresponding to a single Cr unpaired d electron over the whole cell will yield six electrons. The corresponding integrals of $\psi_d\psi_d^*$ and $\psi_p\psi_p^*$ will give six and 18, respectively. If the overlap integral $\int 2\mathrm{Re}\,(\lambda\psi_d\psi_p^*)\,\mathrm{d}v$ is small relative to $1 + \lambda^2$ then the normalization constant $N = \sqrt{1/6(1 + 3\lambda^2)}$. The average moment deficit per 3d orbital is $\Delta\mu = \lambda^2/(1/3 + \lambda^2) = 0.09\ \mu_B$ giving $\lambda \approx 0.18$. This value of λ is of the same order of magnitude as that deduced from neutron diffraction and NMR measurements on other salts containing Cr^{3+} ions [17].

A simple simulation of the charge density associated with a CrO_6 cluster having the same geometry as that in the crystal structure of Cr_2O_3 has been carried out using molecular orbital wavefunctions. This shows that there is strong overlap between the 3d a1 function and the oxygen *p*-functions at the position on the triad axis where the MAXE reconstruction of figure 3 has a significant peak. For $\lambda = 0.18$ the height of the peaks due to overlap are of the same order of magnitude as those in the MAXE difference map. On the other hand the simulated density is much more symmetrical with respect to the Cr site than is that of figure 3. Other peaks due to overlap, in this simulation and those belonging to the e representations, do not correspond very closely to those in the MAXE map although they have much the same size, and occur at much the same distance from the Cr^{3+} ion.

The observation that there is a magnetization gradient at the position of the Cr^{3+} ion has an obvious relevance to the ME effect. Our data refer to the domain in which the spin on the Cr^{3+} ion at $z = 0.34$ points in the direction of positive z. This is the domain in which the spins on the double octahedron (figure 1) point away from their common triangular face. It is the one which is stabilized by cooling in anti-parallel electric and magnetic fields [8]. The sign of ME coefficient which would be predicted from the magnetization gradient $\partial I/\partial z$ at the Cr^{3+} site is consistent with this stabilization. $\partial I/\partial z$ is negative at the Cr^{3+} sites shown in figure 3 and, due to the antisymmetry, has the same sign at all other Cr^{3+} sites. An electric field parallel to positive z would shift the Cr^{3+} ions in the negative z direction, up a magnetization gradient. The consequent increase in magnetic potential favours a reduction in moment of ions with positive relative to those with negative spin, leading to an induced magnetization in the negative z direction. It should however be recalled that the ME coefficient $\alpha_\parallel$ of Cr_2O_3 changes sign at around 100 K [18]. This has been attributed to competition between different mechanisms contributing to the ME effect. The one first proposed by Rado [19] arises from effects

proportional to the product of the sublattice magnetization and the magnetic susceptibility; the former is zero above the Néel temperature and its contribution to the parallel ME effect tends to zero with temperature following $\chi_{\parallel}$. These effects therefore cannot be responsible for either the magnetic annealing effect, or the low-temperature parallel ME effect. A further contribution to the ME effect is that due to the electric field dependence of the spectroscopic splitting tensor and the covalent overlap terms [20, 21]. These latter effects dominate both at low temperature and at the Néel transition, which can explain why the asymmetry of the magnetization distribution in a particular domain at low temperature (25 K) is consistent with that which is energetically favoured by the combination of electric and magnetic fields used to stabilize the domain in the Néel transition.

8. Conclusions

It has been shown that SNP can be used to determine precise values of the magnetic interaction vectors in the class of antiferromagnetic materials in which nuclear and magnetic scattering appear in the same reflections and are in phase quadrature. The method has enabled the magnetization distribution in Cr_2O_3 at 25 K to be determined with good precision.

The distribution can be fitted to a first approximation by a model in which the unpaired electrons are all in those trigonal, a_1 and e, 3d orbitals of the Cr^{3+} ion derived from the cubic orbitals of t_{2g} symmetry. However the total moment associated with each Cr^{3+} ion is only 2.48 μ_B rather than the 2.97 μ_B which would be predicted from the measured g-factor of 1.98. The loss of moment can be attributed to covalent mixing of the Cr 3d electrons with O 2p orbitals in π-type antibonding orbitals. Positive and negative spin transferred to O from oppositely polarized Cr^{3+} ions is superposed and so does not contribute to the magnetization. The magnitude of the moment deficit corresponds to a covalent mixing factor of $\approx$0.18. There are some significant features in the magnetization distribution which are not accounted for by the ionic model; they occur in regions where the Cr and O radial wavefunctions overlap strongly and are hence probably due to covalent overlap.

The magnetization distribution has a gradient at the Cr^{3+} sites which is consistent with a parallel ME coefficient with the same sign as that implied by the combination of magnetic and electric fields needed to stabilize the domain in question.

Acknowledgments

We are grateful to H Humblot for the regular provision of ^{3}He cells during the second part of this experiment and to J Dreyer and E Bourgeat-Lami for providing the means of using them with CRYOPAD on the D3 diffractometer. We should like to thank Dr Nikitas Gidopoulos for helpful discussions on aspects of covalency.

References

[1] Nathans R, Shull C G, Shirane G and Andresen A 1959 *J. Phys. Chem. Solids* **10** 138
[2] Mook H A 1966 *Phys. Rev.* **148** 495
[3] Alperin H A 1961 *J. Phys. Soc. Japan Suppl.* **B-III** 17
[4] Lynn J W, Shirane G and Blume M 1976 *Phys. Rev. Lett.* **37** 154
[5] Wang X L, Stassis C, Johnston D C, Leung T C, Ye J and Harmon B N 1991 *J. Appl. Phys.* **69** 4860
[6] Brown P J, Forsyth J B and Tasset F 1993 *Proc. R. Soc.* A **442** 147
[7] Tasset F, Brown P J, Lelièvre-Berna E, Roberts T, Pujol S, Allibon J and Bourgeat-Lami E 1999 *Physica* B **267/268** 69
[8] Brown P J, Forsyth J B and Tasset F 1998 *J. Phys.: Condens. Matter* **10** 663

[9] Brown P J, Forsyth J B and Tasset F 1999 *Physica* B **267/268** 215
[10] Heil W, Dreyer J, Hofmann D, Humblot H, Lelièvre-Berna E and Tasset F 1999 *Physica* B **267/268** 328
[11] Clementi E and Roetti C 1974 *At. Data Nucl. Data Tables* **14** 182
[12] Sugano S and Peter M 1961 *Phys. Rev.* **122** 381
[13] Hubbard J and Marshall W 1965 *Proc. Phys. Soc.* **86** 561
[14] Papoular R J Vekhter Y and Coppens P 1996 *Acta Crystallogr.* A **52** 397
[15] Corliss L M, Hastings J M, Nathans R and Shirane G 1965 *J. Appl. Phys.* **36** 1099
[16] Samuelsen E J, Hutchings M T and Shirane G 1970 *Physica* **48** 13
[17] Tofield B C 1975 *Structure and Bonding* vol 25 (Berlin: Springer) p 58
[18] Astrov D N 1960 *Sov. Phys.–JETP* **13** 729
[19] Rado G T 1961 *Phys. Rev. Lett.* **6** 609
[20] Royce E B and Bloembergen N 1963 *Phys. Rev.* **131** 1912
[21] Lohr L L and Lipscomb W N 1963 *J. Chem. Phys.* **38** 1607